IL NUOVO CIMENTO **45 C** (2022) 47
DOI 10.1393/ncc/i2022-22047-2

COLLOQUIA: IWM-EC 2021

Temperatures of compound nuclei produced in complete and incomplete fusion and the role of neutron excess

A. B. MCINTOSH(1)(*), K. HAGEL(1), L. A. MCINTOSH(1) and S. J. YENNELLO(1)(2)

(1) *Cyclotron Institute, Texas A&M University - College Station, TX, 77843, USA*
(2) *Chemistry Department, Texas A&M University - College Station, TX, 77843, USA*

received 12 May 2022

Summary. — The role of neutron excess in the nuclear equation of state is important in many systems from the microscopic to the astronomical, and yet the asymmetry energy remains the largest source of uncertainty in the equation of state. We continue our study of the asymmetry dependence of nuclear caloric curve, measuring evaporation of light charged particles from compound nuclei produced Kr + C fusion reactions. The composition and excitation of the compound nuclei are varied by varying the isotope and kinetic energy of the krypton projectile. Temperatures are extracted with kinetic and chemical probes. The more neutron-rich compound nuclei exhibit higher temperatures than the less neutron-rich compound nuclei. We discuss this in light of previous experimental efforts theoretical predictions.

1. – Introduction

The equation of state (EoS) of nuclear matter arises from the microscopic interactions between the constituent particles of the nuclear system. In just a few relevant degrees of freedom, the EoS captures the bulk properties of the nuclear system, relating the temperature, density, pressure, internal energy, and chemical potential for each constituent species. The EoS is relevant from the microscopic to the astronomical: in describing the thermodynamics of heavy-ion collisions in the laboratory, in nucleosynthesis taking place in stellar explosions, in describing the properties of a neutron star from the crust to the core, and in describing collisions of neutron stars (also sites of nucleosynthesis). In all of these arenas, the neutron excess is important [1-4].

The EoS may be studied through the correlation between macroscopic degrees of freedom. One enlightening way is the correlation between the temperature and the excitation energy: the so-called nuclear caloric curve. Early work on the nuclear caloric

(*) E-mail: alanmcintosh@tamu.edu

curve was done by Fabris *et al.* [5], who observed an initial rise in the temperature with increasing excitation energy, followed by a plateau as internal energy increased further. This suggested the possibility of a phase transition, with the analogy in mind of a nuclear liquid boiling or vaporizing into a gas [6].

Subsequent work over the following decades indicated that this was a general phenomenon, with the rise and plateau in the caloric curve qualitatively observed in a wide variety of systems. Different probes, however, produced different quantitative results. Natowitz *et al.* examined a large body of caloric curve data, and after correcting for various systematic effects (*e.g.*, secondary decay) [7] observed that the measured caloric curve data was to a large extent in fact in agreement, provided the data was selected on the size of the system. This provided a demonstration of the mass dependence of the nuclear caloric curve. The lightest systems exhibited a high plateau temperature which was reached at a large excitation; successively heavier systems exhibited successively lower plateau temperatures and onset excitation energies. Natowitz *et al.* explained this feature by Coulomb effects.

If there is a mass (or charge) dependence to nuclear caloric curve, the natural question is whether there is a dependence on the neutron excess. Wuenschel *et al.* [8] sought to probe this in heavy-ion collisions near the Fermi energy, and Sfienti *et al.* [9] sought to probe this at relativistic energies. While both experiments succeeded in measuring temperatures, neither claimed a dependence of the nuclear caloric on the neutron excess of the system, though there were hints that there may indeed be a dependence.

Various theoretical models were used to calculate how the neutron excess might impact nuclear temperatures. The thermal Thomas-Fermi model [10] indicated lower temperatures for more neutron rich systems, as did the Mononuclear model [11]. Contrarily, the hot liquid drop model [12], isospin dependent quantum molecular dynamic model [13], and the statistical multifragmentation model [14] all predict higher temperatures for neutron rich systems.

The clear theoretical predictions that there should be a dependence on neutron excess, the lack of agreement between the models, and the dearth of experimental constraints motivated us to examine the possible asymmetry dependence of the nuclear caloric curve in a new method. We studied heavy-ion collision near the Fermi energy in which multifragmentation is a significant exit channel. We reconstructed the primary excited projectile-like fragment (PLF*) using the isotopically resolved charged particles and measured free neutrons. Correlating the temperature of the PLF* to its deduced excitation energy showed the expected rising trend; by selecting on the neutron excess of the reconstructed PLF*, we showed that the temperatures were systematically lower for more neutron-rich PLF* [15-18]. Knowledge of the composition of the reconstructed PLF*, not the entrance channel composition, was key to observing the dependence on neutron excess. We made a careful study of the impact of the free neutron multiplicity measurement [19], from which we concluded that the observed asymmetry dependence of the caloric curve was not an artifact of the free neutron measurement.

2. – Experimental design and methods

Having observed a dependence of temperature on neutron excess, we aim to measure such a dependence again in a different system with a different reaction mechanism, and with a different detection apparatus. The present experiment is designed to focus on fusion-evaporation in inverse kinematics. In such a mechanism, the excitation energy of the compound nuclei may be calculated from kinematics and knowledge of the fraction

of the target that fused with the projectile; the neutron excess of the compound nuclei is controlled by the neutron excess of the projectile, though with fluctuations depending on which target nucleons fuse to the projectile.

The projectiles were chosen to be ^{78}Kr and ^{86}Kr to obtain heavy compound nuclei with significant difference in neutron excess. These were accelerated by the K500 superconducting cyclotron at the TAMU Cyclotron Institute to energies of 15, 25, and 35 MeV/u. While a heavier projectile would have been also interesting, the highest beam energy would no longer have been possible. The target was chosen to be ^{12}C to have high probability of complete fusion, or high fraction of the target fused in incomplete fusion.

The quadrupole triplet spectrometer (QTS) [20] was used to focus the heavy residues as they traveled across a 5.5 m flight path. Their velocity was measured by time-of-flight using parallel plate avalanche detectors. The most forward 0.9° relative to the ideal beam axis was blocked to avoid direct beam. The QTS was tuned for each beam isotope and energy to defocus the beam and preferentially select residues as close to complete fusion as there was significant yield. This corresponded to central magnetic rigidities of 1.10, 1.40, 1.66 Tm for the 15, 25, and 35 MeV/u ^{78}Kr beams, and 1.14, 1.48, and 1.78 Tm for the 15, 25, and 35 MeV/u ^{86}Kr beams.

Light charged particles were measured in the forward array using silicon technology (FAUST). The FAUST [21] is comprised of 68 Si + CsI(Tl) telescopes with coverage between 1.6° and 45.5°. Following an upgrade, the silicon detectors are position sensitive DADL detectors [22, 23]. The signals of the FAUST [24] were amplified with RisCorp (silicon) [25] or ZeptoSystems (CsI(Tl)+PD) [26] charge sensitive amplifiers, and shaped and digitized with the HINP3 ASIC [27] and the XLM-XXV respectively. The gain of the preamplifiers (110 mV/MeV for silicon, and 45 mV/MeV silicon-equivalent for CsI(Tl) + PD) was chosen to focus on light charged particles ($Z = 1, 2$) and lithium isotopes. The calibration of FAUST follows the procedure described previously [23, 24]. Particles incident on the FAUST are identified using the ΔE-E technique. The position of particles on the face of a DADL silicon detector is determined from the resistive charge splitting using the relative difference of the signal amplitudes from two contacts on a common face of the DADL. The position within a detector is known to better than 200 μm [22], and the relative position of the detectors is determined from design specifications and verified with a precision slotted mask [24]. The energy deposited by charged particles in the silicon detector is calibrated relative to a ^{228}Th alpha source; an empirical correction is made [24] to the energy calibration as a function of position to correct for the pulse-shape distortion arising from the capacitive coupling of the uniformly resistive detector faces. An alternate, and more sophisticated, treatment to compensate for this distortion is described by Hannaman and Aslin *et al.* [28].

3. – Results

3˙1. *Particle velocity distribution.* – The two-dimensional laboratory-frame velocity distribution ($v_\perp$ *vs.* $v_\parallel$) of alpha particles measured in the ^{86}Kr @ 35 MeV/u reactions is shown in fig. 1. A clear ring is observed centered on a velocity slightly below beam velocity. The dearth of particles toward the center of the ring is caused by Coulomb repulsion from the compound nucleus. The exponential decrease of yield moving outward from the peak of the ring contains information on the thermal energy in the emitting source; we will return to this subsequently in detail. Sharp cuts in the distribution correspond to the energy required to punch through the silicon and into the CsI (low $v_\parallel$), the angular acceptance of FAUST (low and high $v_\perp$), and the energy required to punch

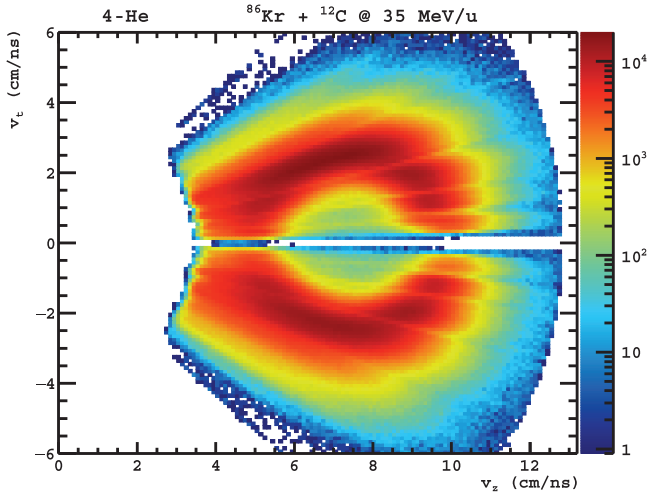

Fig. 1. – Two-dimensional velocity distribution (laboratory frame) of alpha particles produced in reaction of ^{86}Kr +^{12}C @ 35 MeV/u.

through the CsI (high $v_{\|}$). Similar distributions are obtained for other particle types and for other systems.

3˙2. *Residue velocity and compound nucleus excitation energy.* – The velocity of heavy residues detected through the QTS is calibrated using the time-of-flight measurement of the elastically scatted Kr beams and the known flight distance. The velocity distribution of the heavy residues for the ^{86}Kr @ 35 MeV/u is shown in fig. 2. The upper dashed line corresponds to beam velocity and the lower dashed line corresponds to the velocity that would be expected for complete fusion of the Kr with the C target. The distribution

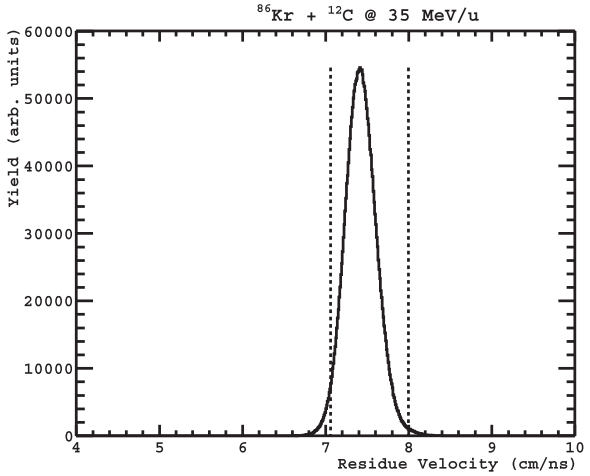

Fig. 2. – Velocity distribution of heavy residues in the laboratory frame. The beam velocity and complete-fusion velocity are indicated by dashed lines.

is peaked closer to the lower line, indicating fusion with more than half of the carbon target. Simple kinematics calculations demonstrate that the width of the distribution is dominated by recoil of the residue in the evaporation process.

Using the measured residue velocity, the kinetic distributions of evaporated particles can be examined, event by event, in the frame of the corresponding measured residue.

Since the width of the residue velocity distribution is broadened event by event, it is not meaningful to use the residue velocity event by event to calculate the excitation energy. However, since the evaporative emission is isotropic, as evidenced by fig. 1, the recoil effect does not alter the mean of the residue velocity distribution, and, hence, this mean velocity can be used to calculate the mean excitation energy for each reaction system.

To calculate the excitation energy, we follow the method of Hagel [29], Fabris *et al.* [5], and Bohne *et al.* [30]. In the present work, the excitation energy is calculated as

$$\frac{E^*}{m_R} = \frac{1}{2}(v_P - v_R)v_R + \frac{Q}{m_R} + \frac{1}{2}\frac{\Delta m_T}{m_R}(\cos(\theta)v_P - v'_T)v'_T, \tag{1}$$

with residue mass m_R, projectile velocity v_P, residue velocity v_R, mass-energy released in breakup Q, unfused mass of the target Δm_T, angle of target remnant θ_T, and velocity of target remnant v'_T; velocities are expressed in the laboratory frame. In the systems in the present study, mass transfer from the light target to the heavy projectile dominates. The first term is the primary kinematic factor, accounting for the change in velocity between the projectile and the compound nucleus, and energy and momentum conservation. The second term is the Q-value of the (complete or incomplete) fusion reaction; for this, the mass of the unfused portion of the target is needed. The third term amounts to a <5% correction for the kinetic energy that the target remnant acquires in the laboratory frame. The mass of the unfused fraction of the target is estimated simply by the relative location of the mean of the residue velocity distribution between beam velocity and the velocity corresponding to complete fusion. In the 15 MeV/u reactions, complete fusion is observed; at 25 MeV/u, two target nucleons on average remain unfused; at 35 MeV/u, four (^{78}Kr) or five (^{86}Kr) target nucleons on average remain unfused.

3˙3. *Kinetic distributions in the frame of the emitting source.* – With knowledge of the residue velocity, it is possible to transform the measured velocity distribution of evaporated particles from the lab frame into the frame of the measured residue, event by event, as an approximation for the frame of the compound nucleus. This is shown in fig. 3 for alpha particles measured in the ^{86}Kr @ 35 MeV/u reactions. This is the same data shown in fig. 1, but with significant loss of data due to the coincidence requirement. In return for loss in counting statistics, the Coulomb ring sharpens substantially. Similar results are obtained for other systems and for other types of evaporated particles. The similarity of the velocity distribution with and without requiring a residue indicates that the ensemble of measured heavy residues is in fact a good representation of the true residue distribution.

The kinetic energy of alpha particles in the frame of their coincident evaporation residue is plotted in fig. 4. In order to obtain the energy spectrum in a way that minimizes the influence of detector acceptance, a cut is placed in velocity space as indicated by the black outlined sector in fig. 3. This corresponds to an angular range of 10° to 70° in the frame of the residues. In fig. 4, the uppermost series of data shows the energy distribution within this angular cut. Each series of data displayed below this uppermost series shows

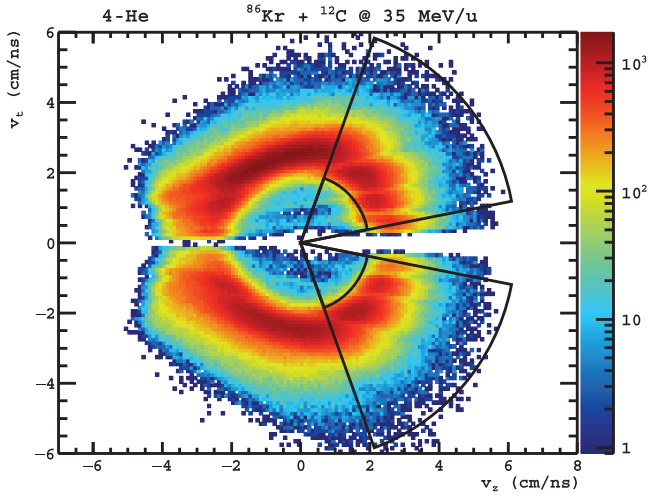

Fig. 3. – Two-dimensional velocity distribution of alpha particles in coincidence with a heavy residue in the residue frame. The sectors indicate the angular range and kinetic range used in fig. 4 for fitting the energy spectra.

the energy distribution for a ten-degree-wide angular range (starting at the top: 0° to 10°, 10° to 20°, etc.); each data series is scaled arbitrarily for visual clarity. The shape of the energy distribution, particularly the exponential slope falling from the high-energy side of the peak, does not depend significantly on the angle within the angular range with full kinematic coverage consistent with isotropic evaporation.

3˙4. *Slope temperature*. – The first method of calculating temperature employed here makes use of the shape of the kinetic energy distributions shown in fig. 4. These are fit with a Maxwell-Boltzmann functional form modified to allow for a diffuse barrier following the prescription of Yanez *et al.* [31]. The result of the fit to the alpha particle energy distribution in the angular range 10° to 70° is shown by the magenta curve in fig. 4. The extent of the magenta line indicates the range of energy considered in the fit. These bounds are also indicated in velocity space in fig. 3 by the sector boundaries. This curve is reproduced and superimposed over the other energy distributions shown below it altering only the overall normalization parameter, emphasizing the fact that the decay is isotropic and the distribution is not distorted by the detector acceptance within this angular region. We take the exponential slope parameter in this fit to be the slope temperature.

The slope temperatures for the six systems are plotted in fig. 5(a) as a function of the excitation energy deduced for each system as described above. The data for the more neutron-rich systems is indicated by the blue data points, and the less neutron-rich systems by the red data points. The error bars in the temperature indicate the uncertainty in the Maxwell-Boltzmann fit (which takes into account the statistical error for each data point). The dominant contribution to the uncertainty in the excitation energy results from the uncertainty in the kinetic energy in the unfused remnant of the target. For both the neutron-rich and neutron-poor compound nuclei, the temperature rises as the excitation energy rises. The neutron-rich system exhibits higher temperatures for all excitation energies than the neutron-poor system.

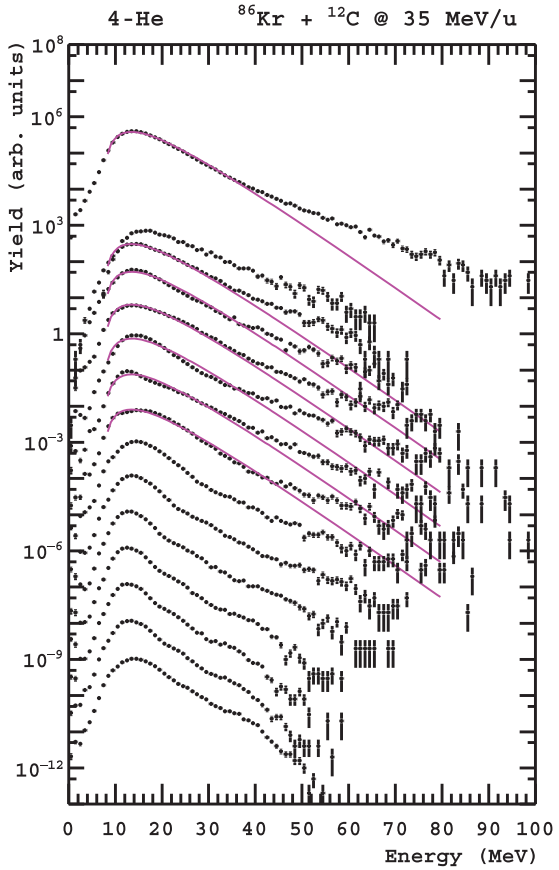

Fig. 4. – Energy distribution of alpha particles measured in coincidence with a heavy residue in the frame of the residue. Upper distribution: $10^\circ < \theta < 70^\circ$. Lower distributions (arbitrarily scaled) from top to bottom: $0^\circ < \theta < 10^\circ$, $10^\circ < \theta < 20^\circ$, etc. The magenta curve is a Maxwell-Boltzmann fit to the uppermost distribution, and scaled and reproduced over other distributions.

3˙5. *Momentum quadrupole fluctuation temperature*. – The classical momentum quadrupole fluctuation thermometer [32] is also a kinetic method, and in principle contains the same information as the slope temperature. The momentum quadrupole is chosen as $Q_{xy} = p_x^2 - p_y^2$, using only transverse components of the momentum to minimize bias from detector acceptance. The quadrupole distribution contains information on the temperature in its width. If it is true that the evaporated particles follow a Maxwell-Boltzmann distribution, as fig. 4 demonstrates they do, the variance of Q_{xy} is related to the temperature by $\langle \sigma_{xy}^2 \rangle = 4m^2T^2$. The temperatures calculated in this way using alpha particles as the probe are shown in fig. 5(b) as a function of the excitation energy. Similarly, the MQF temperatures using protons as the probe particle are shown in fig. 5(c) as a function of excitation. Independent of the neutron richness, a rise of the temperature is seen with increasing excitation. Still, the temperature is higher for the more neutron-rich compound nuclei. The temperatures observed for protons are significantly lower than those for alpha particles at these excitation energies, consistent with previous observation [16], suggesting an emission-time ordering.

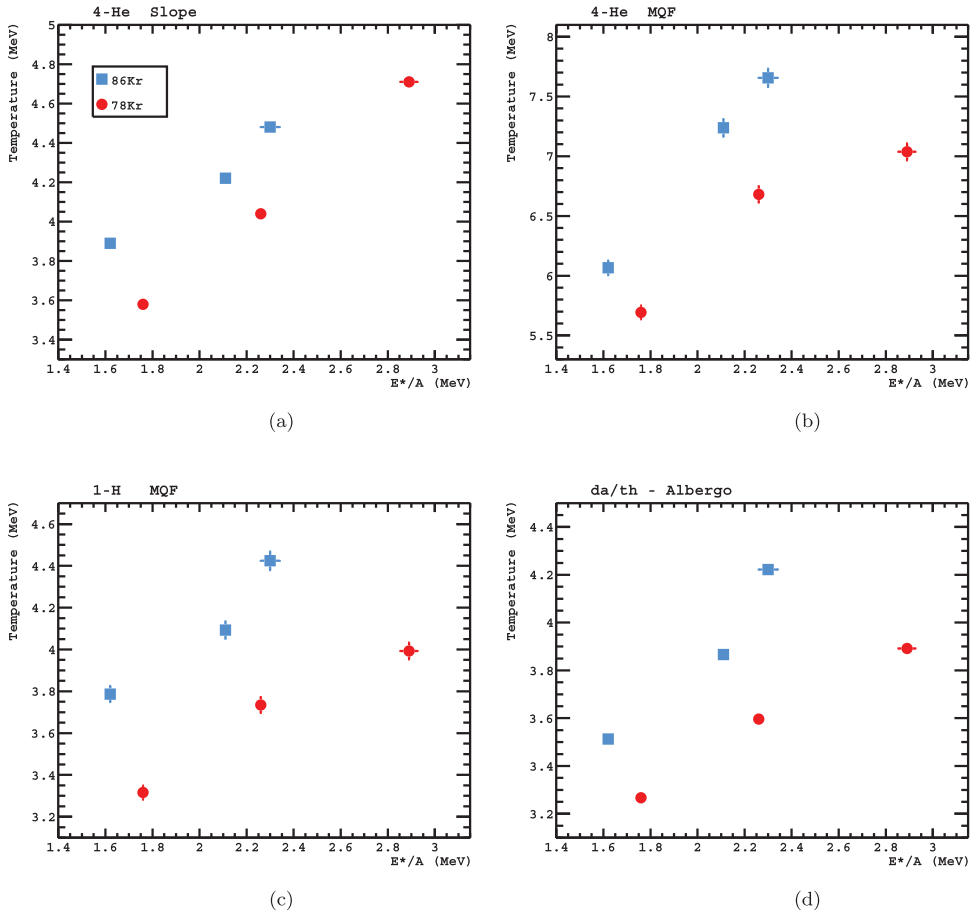

Fig. 5. – Temperature calculated using exponential slope for alpha particles (a), fluctuation method ((b) alpha particles, (c) protons) and (d) Albergo chemical method as a function of excitation energy.

3˙6. *Chemical temperature*. – A chemical approach to extracting the temperature is also employed. The prescription of Albergo *et al.* [33] describes the yield of particular clusters of nucleons in equilibrium as arising from the ground state binding energies and spin degeneracies according to $T_{raw} = \frac{B}{\ln(aR)}$ where B is a double difference of binding energies, a is a double ratio of spin degeneracies, and R is a double isotopic yield ratio. We include a correction for secondary decay as described by Xi *et al.* [34] as $T = \frac{1}{\frac{1}{T_{raw}} - \frac{\ln(\kappa)}{B}}$. It is understood that certain kinetic thermometers may differ from chemical thermometers due to a variety of factors such as the Fermi motion of nucleons (see, *e.g.*, refs. [35, 36]). The temperatures deduced with this chemical approach when using d, t, h, α for the double ratio are shown as a function of the excitation energy in fig. 5(d). Here, too, the temperature increases with increasing excitation energy; and again the temperatures extracted for neutron-rich compound nuclei are higher than those for the neutron-poor compound nuclei.

4. – Discussion of results and future directions

Temperatures for compound nuclei have been extracted experimentally using light charged particle probes and employing both kinetic and chemical thermometers. The excitation energy was varied by varying the beam energy, and the composition of the compound nuclei varied by varying the beam isotope. The temperatures for the neutron-rich compound nuclei are higher than for the neutron-poor compound nuclei. This is in tension with our previous results studying multi-fragmentation reactions [15-17]. In the present data, we are considering compound nuclei with similar atomic number, while in our previous study we considered a narrow range of mass number; this convolutes the mass dependence observed by Natowitz *et al.* [7] (ascribed to Coulomb effects) with the asymmetry dependence, though the magnitude of this should be quite small given the ranges of mass and atomic number. It may be important to account accurately the effects of sequential decay, and extract primary temperatures rather than average cascade temperatures. Since the emission order of particle type may depend, through changes in Q value, on the composition of the source, the cascade temperatures in either or both the multi-fragmentation and fusion data may be masking the true asymmetry dependence of the nuclear caloric curve. It is possible that Coulomb corrections to the thermometers may impact the extracted temperatures for the different systems to different extents; this may have a stronger effect in the multi-fragmentation reactions where the mass was held constant and the relative neutron excess allowed to vary. If differences in the ordering of the caloric curve by neutron-richness persist after applying Coulomb corrections and accounting for sequential decay, differences in the ordering may reflect different physics in the reaction mechanism: the multi-fragmentation explores lower density than fusion-evaporation. Besides changing emission barriers, this also impacts the binding energy of the clusters themselves [37], and changes the magnitude of the nucleon effective mass splitting and the magnitude of the symmetry energy relevant to the reaction. While our understanding of the asymmetry dependence of the nuclear caloric curve is far from complete, it is nevertheless encouraging to see, in a second system, a dependence of nuclear temperatures on the neutron excess. Now the complications and subtleties can begin to be systematically addressed.

* * *

We thank the staff of the TAMU Cyclotron Institute for providing the high quality beams which made this experiment possible. This work was supported by the Robert A. Welch Foundation (A-1266), and the U. S. Department of Energy (DE-FG02-93ER-40773). We thank Lee Sobotka for supplying the HINP ASIC, the development of which was supported by the U. S. Department of Energy (DE-SC0004972).

REFERENCES

[1] Janka H. T. *et al.*, *Phys. Rep.*, **442** (2007) 38.
[2] Danielewicz P., Lacey R. and Lynch W. G., *Science*, **298** (2002) 1592.
[3] Li B. A., Chen L. W. and Ko C. M., *Phys. Rep.*, **464** (2008) 113.
[4] Lattimer J. M. and Prakash M., *Science*, **304** (2004) 536.
[5] Fabris D. *et al.*, *Phys. Lett. B*, **196** (1987) 429.
[6] Viola V. and Kwiatkowski K., *Am. Sci.*, **86** (1998) 449.
[7] Natowitz J. B. *et al.*, *Phys. Rev. C*, **65** (2002) 034618.
[8] Wuenschel S. *et al.*, *Nucl. Phys. A*, **843** (2010) 1.

[9] Sfienti C. *et al.*, *Phys. Rev. Lett.*, **102** (2009) 152701.
[10] Kolomietz V. M., Sanzhur A. I., Shlomo S. and Firin S. A., *Phys. Rev. C*, **64** (2001) 024315.
[11] Hoel C., Sobotka L. G. and Charity R. J., *Phys. Rev. C*, **75** (2007) 017601.
[12] Besprosvany J. and Levit S., *Phys. Lett. B*, **217** (1989) 1.
[13] Su J. and Zhang F. S., *Phys. Rev. C*, **84** (2011) 037601.
[14] Ogul R. and Botvina A. S., *Phys. Rev. C*, **66** (2002) 051601(R).
[15] McIntosh A. B. *et al.*, *Phys. Lett. B*, **719** (2013) 337.
[16] McIntosh A. B. *et al.*, *Phys. Rev. C*, **87** (2013) 034617.
[17] McIntosh A. B. *et al.*, *Eur. Phys. J. A*, **50** (2014) 35.
[18] McIntosh A. B. and Yennello S. J., *Prog. Part. Nucl. Phys.*, **108** (2019) 103707.
[19] Marini P. *et al.*, *Nucl. Instrum. Methods A*, **707** (2012) 80.
[20] Cammarata P. *et al.*, *Nucl. Instrum. Methods A*, **729** (2015) 61.
[21] Gimeno-Nouges F. *et al.*, *Nucl. Instrum. Methods A*, **399** (1997) 94.
[22] Soisson S. N. *et al.*, *Nucl. Instrum. Methods A*, **613** (2010) 240.
[23] McIntosh L. A. *et al.*, *Nucl. Instrum. Methods A*, **985** (2021) 164642.
[24] Heilborn L. A., PhD Thesis, Texas A&M Univ. (2018).
[25] Todd R., Ris-corp, 5905 Weisbrook Lane, Suite 102 Knoxville, TN 37909.
[26] de Souza R., Zeptosystems, Bloomington, IN 47401.
[27] Engel G. *et al.*, *Nucl. Instrum. Methods A*, **573** (2007) 418.
[28] Aslin M. *et al.*, *Nucl. Instrum. Methods A*, **985** (2021) 164674.
[29] Hagel J. C., PhD Thesis, Texas A&M Univ. (1896).
[30] Bohne W. *et al.*, *Phys. Rev. C*, **41** (1990) R5.
[31] Yanez R. *et al.*, *Phys. Rev. C*, **68** (2003) 011602(R).
[32] Zheng H. and Bonasera A., *Phys. Lett. B*, **696** (2011) 178.
[33] Albergo S., Costa S., Costanzo E. and Rubbino A., *Nuovo Cimento*, **89** (1985) 1.
[34] Xi H., Lynch W. G., Tsang M. B., Friedman W. A. and Durand D., *Phys. Rev. C*, **59** (1999) 1567.
[35] Bauer W., *Phys. Rev. C*, **51** (1995) 803.
[36] Kelic A., Natowitz J. B. and Schmidt K. H., *Eur. Phys. J. A*, **30** (2006) 203.
[37] Hagel K. *et al.*, *Phys. Rev. Lett.*, **108** (2012) 062702.